Role of Protein and Substrate Dynamics in Catalysis by *Pseudomonas putida* Cytochrome $P450_{cam}$[†]

Swati Prasad*,[‡] and Samaresh Mitra

Department of Chemical Sciences, Tata Institute of Fundamental Research, Homi Bhabha Road, Colaba, Mumbai-400005, India

Received July 1, 2002; Revised Manuscript Received September 10, 2002

ABSTRACT: The role of protein structural flexibility and substrate dynamics in catalysis by cytochrome P450 enzymes is an area of current interest. We have addressed these in cytochrome $P450_{cam}$ ($P450_{cam}$) and its Y96A mutant with camphor and its related compounds using fluorescence spectroscopy. Previously [Prasad et al. (2000) *FEBS Lett. 477,* 157−160], we provided experimental support to dynamic fluctuations in $P450_{cam}$, and substrate access into the active site region via the channel next to the flexible F−G helix−loop−helix segment. In the investigation described here, we show that the dynamic fluctuations in the enzyme are substrate dependent as reflected by tryptophan fluorescence quenching experiments. The orientation of tryptophan relative to heme (κ^2) for W42 obtained from time-resolved tryptophan fluorescence measurements show variation with type of substrate bound to $P450_{cam}$ suggesting regions distant from heme-binding site are affected by physicochemical and steric characteristics/protein−substrate interactions of $P450_{cam}$ active site. We monitored substrate dynamics in the active site region of $P450_{cam}$ by time-resolved substrate anisotropy measurements. The anisotropy decay of substrates bound to $P450_{cam}$ indicate that mobility of substrates is modulated by physicochemical and steric characteristics/protein−substrate interactions of local active site structure, and provides an understanding of factors controlling observed hydroxylated products for substrate bound $P450_{cam}$ complexes. The present study shows that $P450_{cam}$ local and peripheral structural flexibility and heterogeneity along with substrate mobility play an important role in regulating substrate binding orientation during catalysis and accommodating diverse range of substrates within $P450_{cam}$ heme pocket.

Cytochrome P450 enzymes (P450s)[1] are heme protein monooxygenases that metabolize a wide variety of physiologically important compounds vital to life of most organisms from protists to plants to man (*1*). P450s monooxygenate multitude of substrates that are involved in physiologically important processes such as steroid metabolism, procarcinogen activation, fatty acid metabolism, and xenobiotic (drug and pollutant) detoxification (*1*, *2*). Such broad substrate diversity and the structural determinants for substrate specificity/product control in P450s remain among the critical unresolved questions in P450s. Understanding of substrate specificity/product control in P450s is very important in deciding whether a specific compound will be a substrate for a given P450 enzyme, or for the design and construction of P450 enzymes with tailored substrate specificities, and for the prediction of potential toxic interactions. Several studies have attempted to understand the factors, such as structural flexibility/dynamics and substrate mobility, that might control substrate binding orientation during catalysis and accommodation of diverse range of substrates within P450 heme pocket (substrate diversity). Interestingly, topology, structural fold, and the heme-binding core structure among microbial and mammalian P450s (*3*, *4*) seem to be conserved along with structural constraints for restricted water access to heme to avoid conversion of activated dioxygen to superoxide or peroxide during catalysis. The regions associated with substrate binding and recognition in P450s are believed to be helices A, B, B′, F, and G and their adjacent loops (*5*). The mutation of amino acid residues within these regions has been shown to confer new substrate specificities onto P450s or alter its stereo- and regioselectivity (*1*, *6*). Very recently, Winn et al. (*9*) based on molecular dynamic simulation studies proposed that the substrate access channel to the P450 active site may dynamically modulate substrate binding. The crystal structures of $P450_{terp}$ and P450 2C5 show disorder/flexibility in the F−G region (*4*, *7*). Recently, Dunn et al. (*8*) showed using ruthenium-linker substrates bound to $P450_{cam}$ that large changes in peripheral enzyme structure (F and G helices) are coupled to conformational changes in the active site residues (I helix) and flexibility in the F/G helix region. Such structural flexibility in P450s is thought to be the reason for its observed substrate diversity.

A paradigm for the structural understanding of P450s is the soluble camphor-metabolizing cytochrome $P450_{cam}$ isolated from *Pseudomonas putida*. $P450_{cam}$ is a 45 kDa polypeptide chain containing a single ferric protoporphyrin IX, where the heme iron (III) is hexacoordinated with a water

[†] This research was supported by Tata Institute of Fundamental Research, Mumbai, India.

* To whom correspondence should be addressed.

[‡] Present address: Department of Biochemistry and Molecular Biophysics, Washington University School of Medicine, Box 8231, St. Louis, MO 63110. Tel: 314-362-4187. Fax: 314-362-7183. E-mail: prasad@biochem.wustl.edu.

[1] Abbreviations: cytochrome $P450_{cam}$ ($P450_{cam}$), diethyl aminoethyl (DEAE), quatenary ammonium (Q), *N*-acetyltryptophanamide (NATA).

10.1021/bi026379e CCC: $22.00
Published on Web 11/09/2002

molecule and S atom of Cys-357 in the fifth and sixth coordination positions, respectively (*10*, *11*). $P450_{cam}$ catalyzes the stereo- and regiospecific hydroxylation of camphor to 5-exo-hydroxycamphor at the expense of one mole each of NADH and dioxygen (*12*). In addition to camphor derivatives and the closely related tricyclic molecules adamantane and adamantanone, $P450_{cam}$ has been shown to oxidize unrelated compounds such as styrene and its derivatives, ethylbenzene, nicotine, and polycyclic aromatic hydrocarbons such as naphthalene and pyrene (*1*, *13*). It is likely that such substrate diversity for $P450_{cam}$ arises due to protein structural flexibility, such that $P450_{cam}$ can be modified to accommodate various substrates in multiple orientations. Recently (*14*), we successfully utilized the intrinsic fluorescence of the indole moiety of tryptophan residue to provide experimental support to structural flexibility/dynamic fluctuations in $P450_{cam}$ and substrate access into the active site region via the channel next to the flexible F−G helix−loop−helix segment. Among the five tryptophan residues in $P450_{cam}$, W42 is closest to the substrate access channel located between the B′ helix and the flexible F−G helix−loop−helix segment. Thus, the fluorescence properties of W42 residue in the presence of substrates with varied physicochemical/protein−substrate interaction of $P450_{cam}$ active site can provide information on the effect of local active site structure in regulating structural flexibility/fluctuations involving entry/passage of the substrate through the access channel. Considering this, we investigated the structural flexibility of $P450_{cam}$ in various substrate (substrates: norcamphor, thiocamphor, fenchone, and adamantone) bound forms and camphor-bound Y96A $P450_{cam}$ using tryptophan fluorescence spectroscopy.

The crystal structure of $P450_{cam}$ has been solved at high resolution in the substrate-free form, and in the forms in which the enzyme is bound to a number of substrates and inhibitors (*1*, *11*, *15*, *16*). The crystal structure shows that camphor binds in the heme pocket in a single and ordered conformation and various protein−substrate interactions, namely, hydrogen bonding between the camphor carbonyl oxygen and the hydroxyl group of tyrosine 96, specific hydrophobic contacts between the methyl groups of camphor and valine 295, 247, place 5-position of camphor skeleton above the heme iron. Removal of these interactions by either mutating specific amino acids on the enzyme or appropriate substitution of substrate leads to hydroxylated products at multiple positions (*1*, *17*, *18*). The substrate mobility in the active site region of the enzyme has been proposed to play an important role in positioning the substrate within the active site and determining regiospecificity of substrate hydroxylation (*19*, *20*). The involvement of the mobility of substrates in P450 catalytic function has been proposed based on kinetic analysis of the hydroxylation involving deuterium kinetic isotope effects (*21*), deuterium magic angle spinning studies (*22*), high pressure (*23*), and FTIR studies on CO bound P450s (*24*). Substrate docking algorithms and molecular dynamics simulation studies (*19*, *20*, *25*, *26*) propose a degree of plasticity in $P450_{cam}$ active site and substrate motions, to control substrate hydroxylation and for accommodating a diverse range of substrates within the active site. Even though substrate mobility in $P450_{cam}$ has been the subject of several studies (*19*−*26*), direct observation of substrate motion and possible correlation of substrate mobility to product control in $P450_{cam}$ has not been reported so far. Camphor and its related compounds (norcamphor, adamantone, and fenchone) are fluorescent (*27*). The depolarization of fluorescence of organic molecules in liquids is one of the powerful techniques for the investigation of the tumbling or rotational motion of the molecule on the picosecond to nanosecond time scale (*28*). The time-resolved fluorescence anisotropy directly monitors the reorientation of the emission transition dipole moment of the fluorophore and hence is best suited for the investigation of its local molecular dynamics near the active site. The stereo- and regiospecificity for the substrate hydroxylation in $P450_{cam}$ is likely to be dependent on the rotational freedom of the substrates (camphor, adamantone, thiocamphor, norcamphor, and fenchone) and its potential for multiple binding orientations. In view of this, we utilized the fluorescence properties of camphor and related compounds to probe the local environment of the substrate and its dynamics in $P450_{cam}$. In the present work, the fluorescence properties of both tryptophan and substrate in $P450_{cam}$ provide information on the role of protein and substrate dynamics in regulation of substrate hydroxylation, diversity, and product control for this enzyme.

MATERIALS AND METHODS

Materials. DEAE Sepharose, Q Sepharose, Sephadex G10 column, NATA, acrylamide, norcamphor, thiocamphor, adamantone, and fenchone were purchased from Sigma-Aldrich Co. Potassium iodide was obtained from E. Merck. All other chemicals were of analytical grade.

Protein Purification. The recombinant forms of *Pseudomonas putida* $P450_{cam}$ were overexpressed in *Escherichia coli*, and purified according to the reported method (*29*). The enzyme preparation was stored at −20 °C in 1 mM camphor and 40 mM phosphate, pH 7.4 solution containing 50% glycerol.

Steady-State Fluorescence Spectroscopy. Steady-state fluorescence measurements were done on Spex Fluorolog-1681T spectrofluorometer. The fluorescence excitation wavelength was kept at 295 nm and the measured fluorescence intensity (F_{obs}) after the addition of a quencher was corrected for the enzyme dilution and inner filter effect as described earlier (*30*). The tryptophan fluorescence quenching experiments were performed using acrylamide (neutral quencher) and potassium iodide (ionic quencher) as described earlier (*14*, *31*).

Time-Resolved Fluorescence Spectroscopy. The time-resolved fluorescence lifetime and anisotropy decay measurements were carried out on a time-correlated single photon counting device coupled with a picosecond laser described elsewhere (*32*). The exciting laser source was frequency tripled output (885 nm, fundamental) of a mode locked picosecond Ti-sapphire (Tsunami Spectra Physics, USA) laser pumped by a diode pumped CW Nd-Vanadate laser (532 nm) (Millennia X, Spectra Physics, USA). The pulse width of the exciting laser pulse was typically 1−2 ps. A pulse repetition of 82 MHz was reduced to a repetition rate of 800 kHz/4 MHz using a pulse selector (model 3985 Spectra Physics USA) for our measurements. The ultraviolet beam at 295 nm excited the samples. A Schott WG 320 cutoff filter was used to remove any scattering from samples at wavelengths below 320 nm. The instrument response function (IRF) was recorded using a nondairy creamer

scattering solution and the apparatus response was checked by measuring the lifetime of NATA, before the start of sample data acquisition. Protein samples (~10 μM) in 40 mM, pH 7.4 potassium phosphate buffer were used for the time-resolved fluorescence measurements. For fluorescence lifetime measurements, the emission profiles were collected from the sample through the emission polarizer oriented at the magic angle (54.7°) with respect to the excitation polarizer to avoid any contribution from anisotropy. For time-resolved anisotropy experiments, fluorescence decays were collected with the emission polarizer kept at parallel ($I_{||}$) and perpendicular ($I_{\perp}$) orientations with respect to the excitation polarizer. These polarized components were corrected for the G factor of the instrument. G factors for the different emission wavelengths were determined by the tail-matching method (*33*) using NATA for which the rotational correlation time (~56 ps) is much faster than its fluorescence lifetime (~3 ns). G factor for the protein samples were measured by collecting $I_{\perp}$ for the time, $t_{||} \times$ G, where $t_{||}$ is the time for which $I_{||}$ was collected.

The fluorescence decay curves were analyzed by the best fit to the deconvolution of instrument response function with a theoretical decay function composed of a discrete sum of exponentials, given by the following equation:

$$I(t) = \sum_k \alpha_k \exp(-t/\tau_k) \tag{1}$$

where k is the number of discrete exponentials required to fit the emission profile. To obtain the amplitudes (α_k) and lifetimes (τ_k), an iterative reconvolution was applied using nonlinear regression and Marquardt's algorithm for parameter optimization (*34*). The goodness of the fit was confirmed from the randomness of the weighted residual distribution, autocorrelation function and with a χ^2 value close to unity.

The fluorescence decay profiles were also analyzed independently by the maximum entropy method (MEM) using 150 lifetime components ranging from 0.01 to 10 ns uniformly distributed in the logarithmic time scale. This method is an unbiased way of data analysis in the sense that it provides a continuous distribution of lifetimes without assuming any model or mathematical function (*35*). MEM initially starts with a flat distribution of amplitudes; that is, each lifetime has equal weighting in the beginning and arrives at the amplitude distribution that best describes the observed experimental fluorescence intensity decay. The optimization of the amplitude distribution is carried out in successive cycles by minimizing the χ^2 and maximizing the entropy, S. The expression used for S is the Shannon-Jaynes entropy function (*36*), which is

$$S = -\sum p_i \log p_i \tag{2}$$

where $p_i = \alpha_i / \sum \alpha_i$.

Fluorescence resonance energy transfer (FRET) is a distance-dependent excited-state dipole−dipole interaction in which the emission of one of the fluorophore (donor) is coupled to the excitation of another (acceptor). It occurs primarily because the acceptor dipole interacts or resonates with the donor dipole. FRET can be used to estimate the distance of the fluorophore from the acceptor group. The efficiency of energy transfer (E) depends on the distance (R) and the relative orientation of donor and acceptor (*30*, *37*), and is related by eq 3:

$$E = \frac{R_o^6}{R^6 + R_o^6} = 1 - \frac{\tau_{da}}{\tau_d} \tag{3}$$

where τ_{da} and τ_d represent the lifetime of donor in the presence and in the absence of acceptor, respectively. R_o is the distance for 50% energy-transfer efficiency. R_o was calculated using the following relation:

$$R_o = (J \kappa^2 Q_d n^{-4})^{1/6} \times 9.79 \times 10^3 \text{ Å} \tag{4}$$

where J is the spectral overlap integral of the normalized emission spectrum of the donor (tryptophans) and absorption spectrum of the acceptor (heme), and was calculated by the reported method (*38*). n ($n = 1.4$) is the refractive index of the medium. Q_d is the quantum yield of tryptophan ($Q_d = 0.13$) in absence of any quencher (*31*). κ^2 is the orientation factor of the tryptophan-heme transition moments and is defined by the direction of the transition moment of the donor (tryptophan) and acceptor (heme). It varies from 0 to 4 depending upon their relative orientation (*30*). κ^2 can be computed for the heme proteins using their atomic coordinates, and the experimentally observed lifetimes can be correlated to the structural disposition of their tryptophan residues (*39*).

The analysis of time-resolved fluorescence anisotropy decay $r(t)$ was carried out using the two polarized decays, $I_{||}$ and $I_{\perp}$ collected with the emission polarizer oriented parallel and perpendicular to the excitation polarizer (*40*). These two polarized decays are related to the total intensity decay $I(t)$ and the anisotropy decay $r(t)$ according to the following equations:

$$I_{||}(t) = \frac{1}{3} I(t)[1 + 2r(t)] \tag{5}$$

$$I_{\perp}(t) = \frac{1}{3} I(t)[1 - r(t)] \tag{6}$$

Here, the intensity decay $I(t)$ is a multiexponential function given by eq 1. The fluorescence anisotropy in the case of proteins comes from two independent motions: rotational dynamics of the entire protein (global motion) and segmental dynamics of the fluorophore (local motion). Assuming that the segmental motions occur independent of the overall protein rotation, the anisotropy decay function $r(t)$ can be represented as the product of these separate processes (*40*). Anisotropy decay function $r(t)$ that was used to analyze the experimental anisotropy data is expressed by eq 7.

$$r(t) = r_0 \sum_i f_i \exp(-t/\phi_i) \tag{7}$$

where r_0 is the time zero anisotropy (initial anisotropy), which can vary between 0.4 and −0.2; ϕ_i ($i = 1$ and 2) are the rotational correlation times associated with the "local" and "global" rotations, respectively, and f_i ($i = 1$ and 2) are the fractional changes in anisotropy associated with ϕ_1 and ϕ_2, respectively. Goodness of the fit was determined based on random distribution of the weighted residuals, χ^2 value,

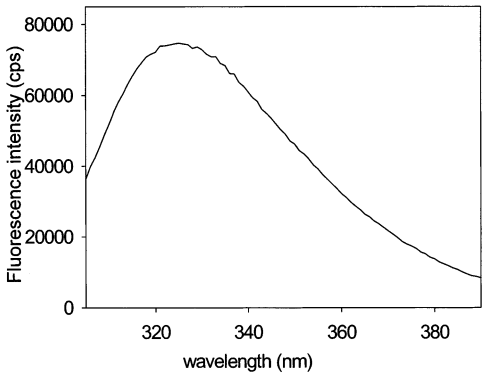

FIGURE 1: Steady-state tryptophan fluorescence spectra of 5 μM adamantone-bound cytochrome P450$_{cam}$ in 40 mM, pH 7.4 phosphate buffer. Excitation wavelength was kept at 295 nm.

Table 1: Fluorescence Parameters for Camphor and Related Compounds in Ethanol[a]

Substrates	λ_{ex} *(nm)*	λ_{em} *(nm)*	τ_f *(ns)*
Camphor	298	417	3.68
Adamantone	299	420	5.32
Norcamphor	298	420	6.69
Fenchone	300	421	2.34

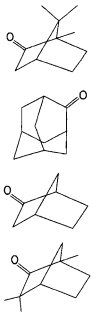

[a] λ_{ex}, λ_{em}: excitation and emission wavelengths; τ_f: fluorescence lifetime.

and a good fit of the calculated anisotropy function with the experimental data.

RESULTS

The tryptophan fluorescence emission spectra of substrate bound P450$_{cam}$ complexes (substrates: camphor, adamantone, thiocamphor, norcamphor, and fenchone) show a broad peak around 325 nm similar to one reported earlier for substrate-free and camphor-bound enzyme (*14*). Figure 1 shows a typical fluorescence emission spectrum for adamantone-bound P450$_{cam}$. Camphor and related compounds (norcamphor, fenchone, adamantone) show weak fluorescence, since it arises due to the carbonyl $n \rightarrow \pi^*$ forbidden transitions (*27*, *41*). The fluorescence emission spectrum of the free substrates, such as camphor, adamantone, norcamphor, and fenchone (Table 1), shifts to 430 nm on their binding to wild-type P450$_{cam}$. Figure 2 shows the typical red shift for camphor emission maxima (from 417 to 430 nm) on binding to wild-type P450$_{cam}$.

The use of quenchers with varying properties such as acrylamide (neutral) and potassium iodide, KI (ionic) can provide information about the environment of the fluorophore. We performed tryptophan quenching experiments on P450$_{cam}$−substrate complex with norcamphor, fenchone, thiocamphor as substrates and camphor-bound Y96A mutant of P450$_{cam}$. The Stern−Volmer (SV) plots for acrylamide quenching in P450$_{cam}$−substrate complexes was found to be

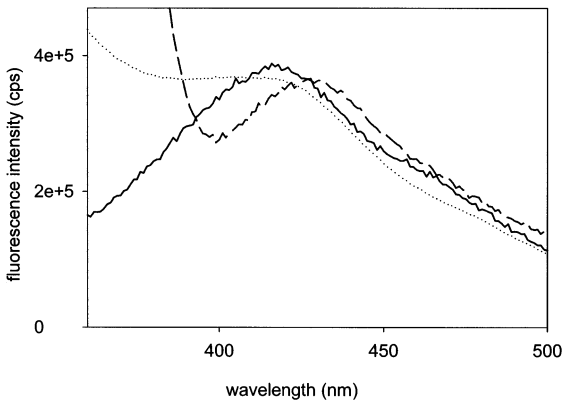

FIGURE 2: Steady-state fluorescence spectra of 9 μM free camphor (solid line), camphor bound to wild-type P450$_{cam}$ (dash line), and camphor bound to Y96A P450$_{cam}$ (dotted line) in 40 mM, pH 7.4 phosphate buffer.

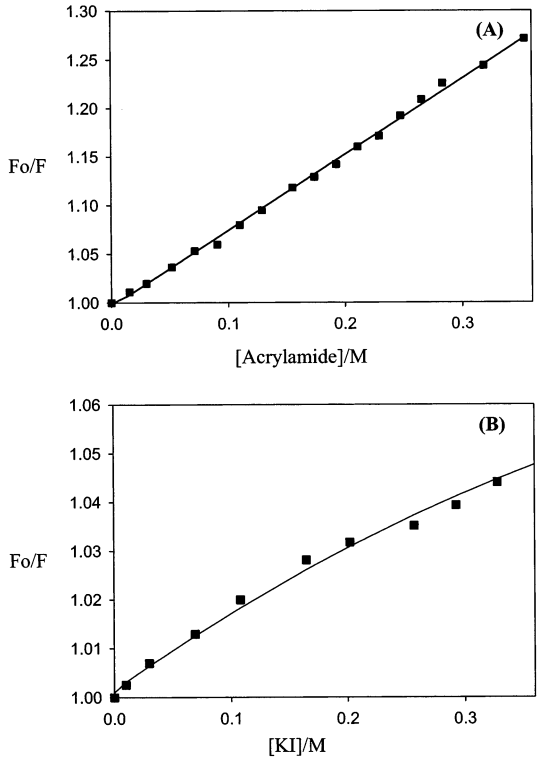

FIGURE 3: Stern−Volmer plots for tryptophan fluorescence quenching of adamantone-bound cytochrome P450$_{cam}$ by acrylamide (A) and KI (B).

linear, whereas that for KI with substrate-bound enzyme shows a downward curvature at higher concentration of KI (Figure 3). The Stern−Volmer constants (K_{SV}), fraction of tryptophan accessible to KI (f_a) and the bimolecular rate constant for acrylamide quenching (k_q) were calculated from SV and Lehrer plots and (*14*, *30*, *31*) are listed in Table 2.

Time-resolved fluorescence studies were carried out to obtain fluorescence lifetimes for both tryptophans and substrates in P450$_{cam}$−substrate complexes. An unusually large Franck−Condon shift (~100 nm) for camphor and its analogues allowed us to measure substrate fluorescence independent of tryptophan. A deconvolution of substrate-bound P450$_{cam}$ fluorescence emission spectrum indicated that emission wavelength around 470 nm had tryptophan fluorescence comparable to background counts. The fluorescence intensity decay for tryptophans (325 nm), free substrate (417

Table 2: Steady-State Fluorescence Quenching Constants[a]

	acrylamide			
$P450_{cam}$	K_{sv} (M^{-1})	$k_q/10^9$ ($M^{-1}\,s^{-1}$)	KI K_{sv} (M^{-1})	f_a
wild-type substrate-free	1.45	5.64	0.13	0.16
wild-type camphor-bound	0.69	2.92	0.21	0.28
wild-type thiocamphor-bound	0.95	4.15	0.32	0.37
wild-type norcamphor-bound	1.21	5.09	0.54	0.49
wild-type fenchone bound	0.93	4.35	0.38	0.41
wild-type adamantone bound	0.81	3.61	0.25	0.31
Y96A camphor-bound	0.92	4.82	0.35	0.32

[a] K_{sv}: Stern−Volmer constant; f_a: fraction of tryptophan accessible to KI.

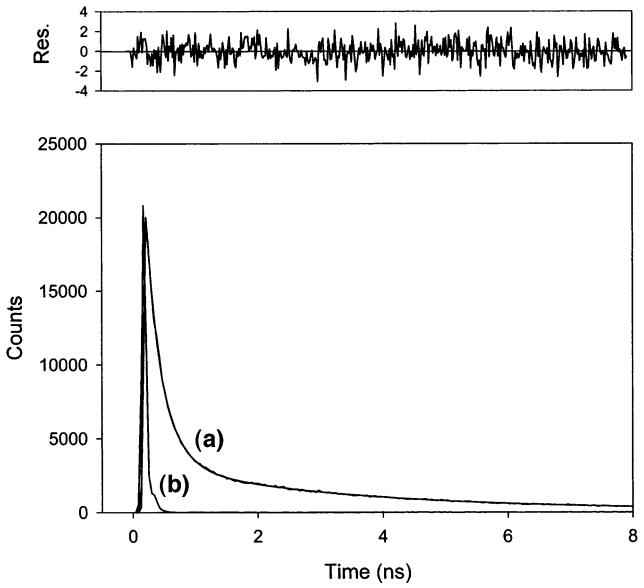

FIGURE 4: Time-resolved decay of camphor in cytochrome $P450_{cam}$ (a) and the instrument response function (b). The solid line through the decay curve shows the four exponential fit. The upper panel in the figure shows the weighted residual [$F_{cal}(t) - F_{exp}(t)$] plot illustrating the accuracy of the exponential fit.

nm), and substrate in $P450_{cam}$-bound forms (470 nm) were collected at magic angle polarization with an excitation wavelength at 295 nm. The fluorescence lifetime for the free substrates (camphor, norcamphor, adamantone, and fenchone) was found to have a single component in the range of 2.3−6.7 ns (Table 1), and the values are in agreement with those reported earlier (*27*). The fluorescence decay curves of the tryptophans and substrates in $P450_{cam}$−substrate complexes were best fitted to a sum of four exponential, as judged by random residual distribution, autocorrelation function, and χ^2 minimization criteria (Figure 4). The decay curves were also analyzed by maximum entropy method (MEM) to check the validity of the discrete exponential model, and the results were found to be in agreement. Figure 5 shows the typical MEM analysis of the substrate fluorescence intensity decay for camphor in $P450_{cam}$. The lifetime components and the amplitudes for the tryptophan and substrates fluorescence are listed in Tables 3 and 4.

We have recently reported (*14*) the assignment of the shortest tryptophan lifetime component (τ_1) in $P450_{cam}$ to W42 by correlating tryptophan disposition relative to heme (κ^2) to its experimentally observed individual lifetime components (using eqs 3 and 4) in camphor-bound $P450_{cam}$. We determined the values of κ^2 for W42 in other $P450_{cam}$-substrate complexes [substrates: adamantone (PDB: 5CPP), norcamphor (PDB: 7CPP) and thiocamphor (PDB: 8CPP)] by the reported method (*14*), and these are listed in Table 5.

We monitored rotational dynamics of camphor and related substrates (norcamphor, adamantone, fenchone) in $P450_{cam}$ and its Y96A mutant. The steady-state anisotropy (r_{ss}) for above substrate-bound $P450_{cam}$ complexes was calculated by computing the integrated area of parallel and perpendicular components of the steady state emission spectra. The initially created anisotropy at zero time (r_o) is observed as r_{ss} in the absence of depolarizing rotational diffusion and is given by the relation

$$r_0 = \frac{2}{5}\left(\frac{3\cos^2\alpha}{2}\right) \qquad (8)$$

where α is the angle between the excitation and emission transition dipoles. The value of r_o varies from 0.4 ($\alpha = 0$) to −0.2 ($\alpha = 90°$) depending on the excitation and emission wavelengths. The typical value of α for substrate like camphor was found to be 47° at 295 nm (excitation) and 417 nm (emission) wavelengths. The value of r_o was measured for all the above substrates in glycerol since glycerol provides a rigid environment and eliminates depolarizing rotational diffusion. The values of r_{ss} and r_o were also calculated from the time-resolved polarized decay data, and the results were in agreement with those obtained from the steady state study. The values of r_{ss} and r_o obtained from steady-state experiment are listed in Table 6.

The fluorescence anisotropy decay of substrates in water and ethanol was observed to be single exponential with a rotation correlation in the range of 35−65 ps. The time-resolved anisotropy decay $r(t)$ for substrates in $P450_{cam}$ could not be described adequately by a single exponential function. Simultaneous analysis of the parallel and perpendicular components for all substrate-bound $P450_{cam}$ complexes using eqs 5 and 6, respectively, satisfactorily fitted with a double exponential rotational correlation model. Figure 6 shows the typical parallel and perpendicular components of time-resolved fluorescence intensity decay of norcamphor in $P450_{cam}$ which were collected by G-factor matching. A two exponential fit to the anisotropy decay is shown as an inset to Figure 6. The values for substrate rotation correlation times with their relative amplitudes are listed in Table 6.

DISCUSSION

The emission maximum for tryptophans in proteins varies from 310 to 360 nm depending on their solvent accessibility and the dielectric constant of the medium (*30*). The observed emission peak position for tryptophans in substrate-bound $P450_{cam}$ complexes indicates a relatively nonpolar average environment around the five tryptophan residues with dielectric constant similar to *p*-dioxane and butyl ether (*42*). Other cytochrome P450s, such as $P450_{BM3}$, P450scc, and $P450_{c21}$ show emission maxima around 330, 332, and 342 nm, respectively (*43*). The fluorescence emission spectrum of camphor and its related compounds exhibit a broad structureless emission with a maximum around 420 nm (Table 1). The observed large difference in energy between the Franck−Condon maxima for absorption and emission in these ketones might arise due to significant differences between the geometry of ground and excited states (*44*). The

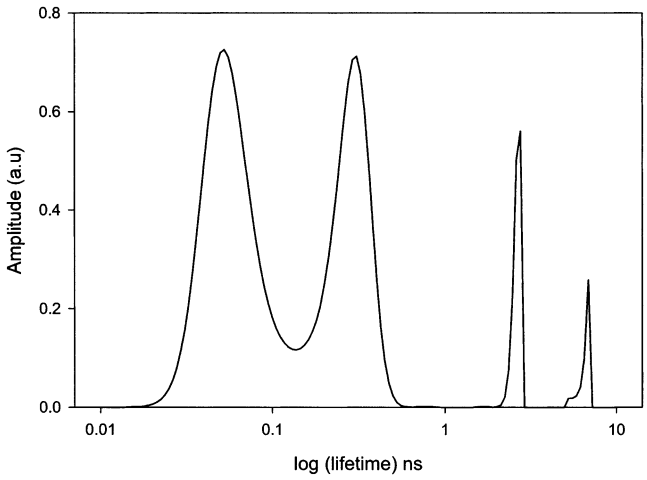

FIGURE 5: Amplitude profile of the distribution of substrate fluorescence lifetimes obtained for best MEM fit of fluorescence decay of camphor in cytochrome $P450_{cam}$.

Table 3: Tryptophan Fluorescence Decay Parameters Recovered by Exponential Analysis[a]

$P450_{cam}$	τ_1 (ns) (amp)	τ_2 (ns) (amp)	τ_3 (ns) (amp)	τ_4 (ns) (amp)	τ_{av} (ns)
wild-type substrate-free	0.126 (57)	0.29 (40)	1.23 (2)	4.47 (1)	0.257
wild-type camphor-bound	0.099 (55)	0.27 (42)	1.18 (2)	4.49 (1)	0.236
wild-type thiocamphor-bound	0.076 (54)	0.28 (43)	1.22 (2)	4.32 (1)	0.229
wild-type norcamphor-bound	0.068 (61)	0.29 (36)	1.20 (2)	4.23 (1)	0.235
wild-type fenchone bound	0.072 (56)	0.26 (41)	1.16 (2)	4.41 (1)	0.214
wild-type adamantone bound	0.100 (52)	0.23 (45)	1.21 (2)	4.52 (1)	0.225
Y96A substrate-free	0.079 (58)	0.28 (39)	1.19 (2)	4.97 (1)	0.229
Y96A camphor-bound	0.045 (63)	0.28 (34)	1.13 (2)	4.5 (1)	0.191

[a] τ (ns): lifetime component; amp: amplitude.

Table 4: Substrate Fluorescence Decay Parameters Recovered by Exponential Analysis[a]

substrate/$P450_{cam}$	τ_1(ns) (amp)	τ_2 (ns) (amp)	τ_3 (ns) (amp)	τ_4 (ns) (amp)
camphor/wild-type	0.065 (51)	0.29 (40)	2.52 (6)	6.4 (3)
adamantone/wild-type	0.069 (51)	0.29 (40)	2.15 (4)	6.2 (5)
camphor/Y96a	0.110 (54)	0.35 (37)	2.31 (6)	6.6 (3)
norcamphor/wild-type	0.096 (54)	0.35 (36)	2.82 (6)	6.3 (3)
fenchone/wild-type	0.106 (57)	0.34 (36)	2.28 (4)	6.6 (3)

[a] τ (ns): lifetime component; amp: amplitude.

spectral distribution of camphor and related compounds shows unusual similarity among themselves (Table 1) and also with other carbonyl compounds (*45*), suggesting that the emission process is localized in their carbonyl moiety. The fluorescence emission spectrum of the free substrates shows a red shift on binding of $P450_{cam}$. This may be attributed to a solvent specific interaction, arising due to hydrogen bonding between carbonyl of the substrate and Tyr 96 in $P450_{cam}$ because emission maximum for camphor in camphor-bound Y96A mutant of $P450_{cam}$ (which lacks a hydrogen bond between carbonyl of camphor and Tyr 96) does not show any red shift relative to emission maxima of camphor (Figure 2), though K_d for camphor in wild-type $P450_{cam}$ (1.1 μM) and Y96A mutant (3.4 μM) are comparable.

Table 5: Tryptophan Orientation Factor (κ^2) for W42 in $P45_{cam}$−Substrate Complex

$P450_{cam}$	κ^2 exp	κ^2 cal
wild-type camphor-bound	0.78	0.75
wild-type adamantone-bound	0.49	0.42
wild-type norcamphor-bound	0.69	0.65
wild-type thiocamphor-bound	0.65	0.62

Table 6: Steady-State and Time-Resolved Fluorescence Parameters for Substrates in Cytochrome $P450_{cam}$[a]

substrate/$P450_{cam}$	ϕ_1(ns) (amp)	ϕ_2 (ns) (amp)	r_o (exp)	r_{ss}(exp)
camphor/wild-type	0.27 (40)	25 (60)	0.084 ±0.004	0.061 ±0.001
adamantone/wild-type	0.28 (45)	26 (55)	0.095 ±0.005	0.072 ±0.001
camphor/Y96A	0.12 (49)	29 (51)	0.12 ±0.01	0.064 ±0.001
norcamphor/wild-type	0.100 (45)	25 (55)	0.106 ±0.003	0.045 ±0.002
fenchone/wild-type	0.112 (47)	24 (53)	0.127 ±0.001	0.060 ±0.001

[a] ϕ_i: rotation correlation time, r_o: initial anisotropy, r_{ss}: steady state anisotropy.

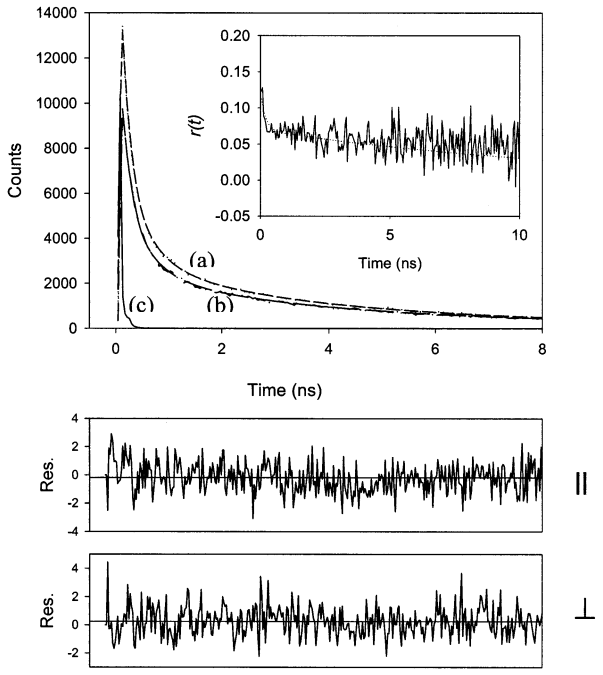

FIGURE 6: Polarized components of fluorescence decay of norcamphor-bound cytochrome $P450_{cam}$: parallel component (a), perpendicular component (b) along with instrument response function (c). The bottom panels show the weighted residuals for the two polarized decays. The anisotropy decay calculated from the two polarized decays is shown in the inset of the figure in the top panel.

The quenching of fluorescence requires molecular contact between the quencher and the fluorophore in either ground or excited state. Fluorescence quenching methods have been extensively used to obtain information on the accessibility of fluorophores to quenchers, ligand binding reactions, conformational changes, dynamic fluctuations in proteins, and protein folding mechanisms (*30*). The Stern−Volmer plots for substrate-bound $P450_{cam}$ complexes (Figure 3) indicate that all five tryptophan residues are accessible to acrylamide, whereas only a fraction of tryptophans is accessible to KI which being an ionic quencher cannot penetrate into the hydrophobic core of the protein. We observe that the fraction of tryptophan accessible to KI increases on binding of substrates to the substrate-free enzyme (Table 2). This suggests that, on binding of substrate to the enzyme, some of the tryptophan residues become accessible to the quencher, as in the case of camphor-bound enzyme (*14*), due to changes in their local environment. Table 2 shows that both K_{sv} and k_q are larger for substrate-free $P450_{cam}$ than for substrate-bound $P450_{cam}$, indicating greater fluctuations in the substrate-free enzyme, which facilitates diffusion of acrylamide inside the enzyme (*46*). On binding of substrates such as thiocamphor (having weak hydrogen bond between carbonyl and Tyr 96), norcamphor (with absence of hydrophobic contacts between substrate 8,9,10-methyl and Leu244−Val247 cleft) or camphor-bound to Y96A $P450_{cam}$ (no hydrogen bond between carbonyl and Y96), the value of both K_{sv} and k_q increase relative to camphor-bound $P450_{cam}$ (Table 2). This indicates that the dynamic fluctuations of the enzyme increase on alteration of active site protein substrate interactions in $P450_{cam}$. It has been shown that alteration of active site protein substrate interactions in $P450_{cam}$ affects both binding of substrate and its hydroxylation (*1*, *17*, *47*). Correlating these to K_{SV} brings out the importance of dynamic properties/flexibility of $P450_{cam}$ in controlling substrate binding and hydroxylation. The observed value of K_{SV} in norcamphor-bound $P450_{cam}$ is much higher than camphor-bound $P450_{cam}$, and is comparable to substrate-free $P450_{cam}$ (Table 2). It has been reported that the enzyme−substrate dissociation constant in norcamphor ($K_D = 150\ \mu M$) is about 100 times larger than camphor ($K_D = 1.1\ \mu M$) (*47*). Also, norcamphor is hydroxylated at multiple positions in contrast to a single hydroxylated product obtained for camphor. Considering these together, larger dynamic fluctuations exhibited by norcamphor-bound $P450_{cam}$ may allow the substrate to attain alternate binding orientations during hydroxylation. The observed substrate dependent dynamic fluctuations (even for closely related substrates) indicate existence of variable and flexible structural states in $P450_{cam}$. This may allow $P450_{cam}$ to accommodate and oxidize different substrates in multiple orientations.

The fluorescence decay for tryptophan residue is known to be multiexponential in single as well as multiple tryptophan containing proteins including several heme proteins (*48*) such as cytochrome *c* oxidase (*49*), HRP (*50*), hemoglobin (*51*), and P450s (e.g., $P450_{BM3}$, P450scc, and $P450_{c21}$) (*43*) attributed to multiple conformations of tryptophan residue in the ground state (*52*) or multiple structures/conformational states of the protein (*53*). Efficient energy transfer between tryptophan and heme dominates the tryptophan fluorescence decay in heme proteins with lifetime components in the subnanosecond range (*37*). Table 3 shows that the two faster lifetime components (τ_1 and τ_2) account for almost 97% of the observed tryptophan fluorescence in substrate-free and substrate-bound $P450_{cam}$. These lifetime components represent a conformation in which the heme and the tryptophan residues are aligned in such a way that the energy transfer to heme is most efficient. The nanosecond lifetime components (τ_3 and τ_4) possibly arise due to presence of small amounts of apoprotein, free substrate, or disordered conformers where tryptophan interactions are different with its neighbors (*54*, *55*). We observe from Table 3 that binding of substrate to substrate-free $P450_{cam}$ greatly decreases the shortest lifetime component (τ_1), the decrease being as large as 64% for camphor-bound Y96A $P450_{cam}$. On the other hand, the other lifetime components are not significantly affected on binding of substrate.

Table 5 shows that the κ^2 for W42 in $P450_{cam}$−substrate complexes match with their reported crystallographic data. This reconfirms that the shortest lifetime component (τ_1) is contributed by W42 and the location of the substrate access channel is between B′ helix and the flexible F−G helix−loop−helix segment, as reported earlier (*14*). Although $P450_{cam}$ bound to camphor and other structurally related compounds are structurally similar, and their trp−heme distances are also similar, a variation in κ^2 for W42 is observed (Table 5). This suggests that the orientation of W42 is affected by the nature of protein−substrate interaction. The regions distant from heme active site are affected by physicochemical and steric characteristics/protein−substrate interactions of $P450_{cam}$ active site, and both local and peripheral enzyme structures are coupled. Similar observation was reported by Dunn et al. (*8*) in ruthenium-linker substrates to $P450_{cam}$, where the authors observe that large changes in peripheral enzyme structure (F and G helices) are coupled to conformational changes in the active site residues (I helix). The observed structural heterogeneity of the local active site and substrate dependent structural flexibility with energetically low-lying structural states for $P450_{cam}$ can be important in regulating binding orientations for substrate during catalysis and accommodating diverse range of substrates in $P450_{cam}$ heme pocket. Such structural flexibility is important since, apart from hydrogen bonding interaction between substrate and Tyr 96, relatively unspecific weak hydrophobic interactions govern the binding of substrates to $P450_{cam}$ in the active site region (*56*).

Our observation of multiexponential fluorescence decay for substrates bound to $P450_{cam}$ (Table 4) indicates conformational heterogeneity in $P450_{cam}$ heme pocket. Table 4 shows that the two faster lifetime components (τ_1 and τ_2) for substrate in the $P450_{cam}$-bound complexes account for almost 91% of the observed substrate fluorescence. The fluorescence decay of heme proteins is dominated by fast energy transfer/decay kinetics (*30*, *37*). Fast energy transfer between substrate and heme will dominate the fluorescence decay of the substrate bound to $P450_{cam}$. Therefore, the fast lifetime components in the subnanosecond range (especially τ_1) arise purely due to bound substrate. However, other lifetime components (τ_3 and τ_4) may not be unambiguously assigned as they are contributed by small amounts of free substrate, apoprotein, or disordered conformers where substrate interactions are different with its neighbors (*54*, *55*). The short lifetime components (τ_1 and τ_2) for camphor in $P450_{cam}$ are similar to those observed for adamantone-bound

$P450_{cam}$. However, these lifetime components substantially increase (as large as 54% in τ_1) on binding of norcamphor, fenchone to wild-type $P450_{cam}$, or camphor to Y96A mutant of $P450_{cam}$. The efficiency of the energy transfer between the substrate and heme will be dependent on their relative distance and orientation (see Materials and Methods). The substrates such as camphor, norcamphor, adamantone, and fenchone are held by Tyr 96 (via hydrogen bonding interaction) in a similar orientation relative to heme (*57*, *58*). Hence, the observed increase in the lifetime components (τ_1 and τ_2) for norcamphor/fenchone bound to wild-type $P450_{cam}$ or camphor to Y96A mutant of $P450_{cam}$ can be attributed to increase in their relative substrate−heme distance. Such an increase in distance has been reported by crystallographic studies (*58*), which show substrates such as norcamphor bind to $P450_{cam}$ about 0.9 Å further from heme than camphor and adamantone.

Fluorescence anisotropy measurements reveal the average angular displacement of fluorophore that occurs between absorption and subsequent emission of a photon, and provide information on the rotational dynamics of the fluorophore. The anisotropy measurements have been extensively utilized in studying denaturation, association, and internal dynamics of proteins (*30*). However, use of such measurements for correlation of enzyme activity and product control to fluorophore (substrate) rotational mobility is rare (*59*).

The fluorescence anisotropy in proteins, characterized by two distinct correlation times, comes from two independent motions: rotational dynamics of the entire protein and segmental/local dynamics of the fluorophore. The local dynamics of the fluorophore can involve fluorophore dynamics with or without a segment of the polypeptide. The local dynamics is generally described by the "wobbling-in-cone" model (60) where the fluorophore can wobble freely within a cone of semi angle related to the order of its environment. Table 6 shows that two types of rotational correlation times define the dynamics of the motion of this system: the one of short correlation time (ϕ_1) ranging from 280 to 100 ps, and the other of large correlation time (ϕ_2) of about 25 ns. The longest correlation time (ϕ_2) in $P450_{cam}$ has been ascribed to the "global" rotational motion of the protein molecule as a whole, and the short correlation times (ϕ_1) to segmental and local dynamics of the substrate in the active site regions of $P450_{cam}$. ϕ_2 can be independently calculated using Stokes−Einstein relation (eq 9) by assuming the shape of the protein to be spherical:

$$\phi_2 = V_h \eta / kT \tag{9}$$

where ϕ_2 is the rotational correlation time, η is the viscosity of the medium, k is the Boltzmann constant, and T is the absolute temperature. V_h is the hydrated molecular volume of the protein, which can be calculated using the following equation 10 (*61*)

$$V_h = \frac{M(\upsilon + h)}{N} \tag{10}$$

where, M is the molecular weight of the protein, N is Avogadro's number, υ is the partial specific volume, and h is the degree of hydration. The value of ϕ_2 was calculated, taking $\upsilon = 0.748$ cm^3/g, $h = 0.2$ cm^3/g, M = 45 kDa, and was found to be 18 ns, which is in agreement with the observed value of 25 ns.

Table 6 shows that the shorter correlation time in $P450_{cam}$ varies with the substrate bound to $P450_{cam}$. However, binding of substrates does not affect the longer correlation time indicating no change in the overall volume or shape of the protein molecule. The short correlation time for camphor bound to $P450_{cam}$ is comparable to adamantone in $P450_{cam}$ but decreases by about 2.6 times in norcamphor and fenchone bound $P450_{cam}$, or when camphor is bound to the Y96A mutant of $P450_{cam}$. This indicates that the internal rotational diffusion of substrate (in the latter case) becomes faster and less hindered. The local mobility in $P450_{cam}$ is therefore substrate dependent, and increases with loss of any of the protein−substrate contacts in $P450_{cam}$. We observe that the regiospecificity of hydroxylation is modulated by combination of interactions, and neither the existence of a hydrogen bond nor the magnitude of van der Waals interactions alone is sufficient to determine the mobility of substrate in active site of $P450_{cam}$. The results were further interpreted in light of available $P450_{cam}$−substrate complex structures (*58*) to rationalize the observed hydroxylated products and product control in $P450_{cam}$. Using the X-ray structural data, the disposition of different amino acid residues in the active site region of camphor, adamantone, and norcamphor bound $P450_{cam}$ is shown in Figure 7. Figure 7a,b shows that $P450_{cam}$ holds both camphor and adamantone in similar rigid configuration. Primary positions (methyl groups) in these substrates are expected to be much less reactive toward hydrogen abstraction. The other positions such as bridgeheads (tertiary carbon) cannot achieve planarity following hydrogen abstraction, making them much less prone to hydroxylation (*17*). Among other positions capable of hydroxylation in camphor, the 3-carbon is α to deactivating carbonyl and the 6-carbon is sterically blocked by the 10-methyl (Figure 7). In adamantone, 4- and 6-carbon secondary positions less reactive than 5-carbon tertiary positions. The restriction in the movement of these substrates due to presence of hydrophobic interactions in addition to the carbonyl hydrogen bond with Tyr 96 in $P450_{cam}$ results in exposure of only the 5-carbon of camphor and adamantone (which is their most reactive position) to the oxyferryl intermediate of $P450_{cam}$, explaining the experimentally observed 100% 5-exo hydroxylated product obtained for them (*17*).

The structural data show that norcamphor has more rotational space in the heme pocket than camphor and adamantone in $P450_{cam}$ (*58*). Table 6 shows that the rate of internal rotational diffusion is smaller for norcamphor relative to camphor and adamantone in $P450_{cam}$ heme pocket, indicating considerable movement of norcamphor during catalysis. $P450_{cam}$ can neither allow truly free and random access of the enzymatic hydrogen abstractor to all parts of norcamphor, nor does it severely restrict its movement; it is anchored to $P450_{cam}$ only through its carbonyl oxygen. The hydrogen bond between norcamphor and Tyr 96 would not be affected by the rotations of norcamphor about the axis passing through and parallel to the carbonyl double bond (Figure 7c). However, any other rotations would necessarily disrupt such anchoring. Considering the rotations in norcamphor along the carbonyl double bond, the oxy-ferryl intermediate of norcamphor-bound $P450_{cam}$ would be exposed its to 3-, 5-, and 6-carbons for hydroxylation. Among

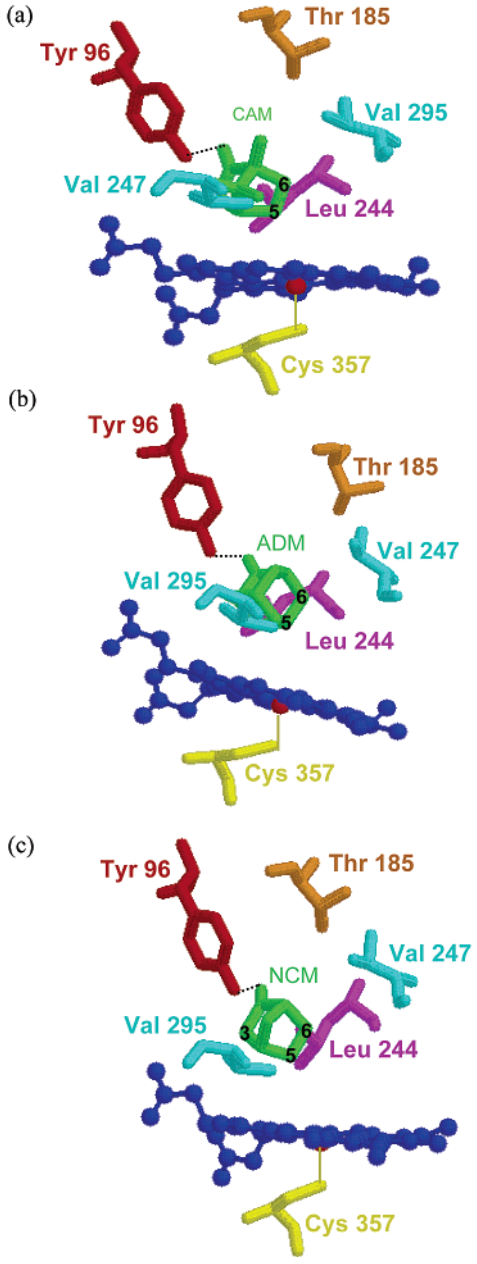

FIGURE 7: Schematic representation of the active site structure of (a) camphor (CAM, PDB code: 2CPP); (b) adamantone (ADM, PDB code: 5CPP); (c) norcamphor (NCM, PDB code: 7CPP)-bound cytochrome P450$_{cam}$ generated from their crystal structure. The location of the hydrogen bond between substrate and Tyr 96 is shown as black dotted line.

these positions, the 3-carbon position is α to deactivating carbonyl and hence is less reactive than the secondary positions 5- and 6-carbons. Since norcamphor is very mobile in the heme pocket, the probability of hydroxylation at both 5-and 6-carbon is almost equal. This provides explanation for the experimentally observed hydroxylated products for norcamphor: 5-exo (45%), 6-exo (47%), and 3-exo (8%) (*18*). The above discussion clearly brings out the importance of substrate mobility in controlling hydroxylation of substrate and product formation in P450$_{cam}$.

CONCLUSIONS

The fluorescence properties of both tryptophan and substrate provide information on the substrate dependent dynamics in P450$_{cam}$. The results show that the dynamic fluctuations in the enzyme are substrate dependent as reflected by tryptophan fluorescence quenching experiments. The observed substrate-dependent structural flexibility can allow this enzyme to accommodate and oxidize diverse range of substrates. The orientation of tryptophan relative to heme (κ^2) for W42 obtained from time-resolved tryptophan fluorescence measurements show variation with type of substrate bound to P450$_{cam}$ suggesting regions distant from heme-binding site are affected by local active site protein−substrate interactions. Both local and peripheral enzyme structures in P450$_{cam}$ are coupled. The anisotropy measurements provide experimental observation of substrate mobility in P450$_{cam}$. The results indicate that mobility of substrates is modulated by local active site structure and provide understanding of factors controlling observed hydroxylated products for substrate-bound P450$_{cam}$ complexes. Time-resolved fluorescence decays for substrates in P450$_{cam}$ suggest structural heterogeneity in P450$_{cam}$, which along with substrate mobility can play an important role in regulating orientations for substrate binding during catalysis and for accommodating diverse range of substrates in P450$_{cam}$ heme pocket.

ACKNOWLEDGMENT

We are grateful to Dr. Luet-Lok Wong, Inorganic Chemistry Lab, Oxford, UK, and Prof. S. Mazumdar for providing us the *E. coli* JM 109 strain containing the gene of interest in pRH1091. We thank Prof. G. Krishnamoorthy and Mr. B. T. Kansara for their help during time resolved fluorescence measurements.

REFERENCES

1. Ortiz de Montellano, P. R., Ed. *Cytochrome P450*: *Structure, Mechanism, and Biochemistry*, Plenum Press, New York 1995.
2. Nelson, D. R., Koymans, L., Kamataki, T., Stegeman, J. J., Feyereisen, R., Waxman, D. J., Waterman, M. R., Gotoh, O., Coon, M. J., Eastabrook, R. W., Gunsalus, L. C., and Nebert, D. W. (1996) *Pharmacogenetics 6*, 1−42.
3. Peterson, J. A., and Graham, S. E. (1999) *Arch. Biochem. Biophys. 369*, 24−29.
4. Williams, P. A., Cosne, J., Sridhar, V., Johnson, E. F., and McRee, D. E. (2000) *Mol. Cell 5*, 121−131.
5. Gotoh, O. (1992) *J. Biol. Chem. 267*, 83−90.
6. Negishi, M., Uno, T., Darden, T. A., Sueyoshi, T., and Pedersen, L. G. (1996) *FASEB J. 10*, 683−689.
7. Hasemann, C. A., Ravichandran, K. G., Peterson, J. A., and Deisenhofer, J. (1994) *J. Mol. Biol. 236*, 1169−1185.
8. Dunn, A. R., Dmochowski, I. J., Bilwes, A. M., Gray, H. B., and Crane, B. R. (2001) *Proc. Natl. Acad. Sci. U.S.A. 98*, 12420−12425.
9. Winn, P. J., Ludemann, S. K., Gauges, R., Lounnas, V., and Wade, R. C. (2002) *Proc. Natl. Acad. Sci. U.S.A. 99*, 5361−5366.
10. Goldfarb, D., Thomann, H., and Ullrich, V. (1996) *J. Am. Chem. Soc. 118*, 2686−2693.
11. Poulos, T. L., Finzel, B. C., and Howard, A. J. (1986) *Biochemistry 25*, 5314−5322.
12. Katagiri, M., Ganguli, B. N., and Gunsalus, I. C. (1968) *J. Biol. Chem. 243*, 3543−3546.
13. England, P. A., Harford-Cross, C. F., Stevenson, J. A, Rouch, D. A., and Wong, L. L (1998) *FEBS Lett. 424*, 271−274.
14. Prasad, S., Mazumdar, S., and Mitra, S. (2000) *FEBS Lett. 477*, 157−160.
15. Poulos, T. L., Finzel, B. C., and Howard, A. J. (1987) *J. Mol. Biol. 195*, 687−700.
16. Dmochowski, I. J., Crane, B. R., Wilker, J. J., and Gray, H. B. (1999) *Proc. Natl. Acad. Sci. U.S.A. 96*, 12987−12990.
17. White, R. E., McCarthy, M. B., Egeberg, K. D., and Sligar, S. G. (1984) *Arch. Biochem. Biophys. 228*, 493−502.

18. Atkins, W. M., and Sligar, S. G. (1989) *J. Am. Chem. Soc. 111*, 2715−2717.
19. De Voss, J. J., Sibbesen, O., Zhang, Z., and Ortiz de Montellano, P. R. (1997) *J. Am. Chem. Soc. 119*, 5489−5498.
20. Das, B., Helms, V., Lounnas, V., and Wade, R. C. (2000) *J. Inorg. Biochem. 81*, 121−131.
21. Atkinson, J. K., Hollenberg, P. F., Ingold, K. U., Johnson, C. C., Le Tadic, M. H., Newcomb, M., and Put, D. A. (1994) *Biochemistry 33*, 10630−10637.
22. Lee, H., Ortiz de Montellano, P. R., and McDermott, A. E. (1999) *Biochemistry 38*, 10808−10813.
23. Jung, C. (2002) *Biochim. Biophys. Acta 1595*, 309−328.
24. Jung, C. (2000) *J. Mol. Recognit. 13*, 325−351.
25. Audergon, C., Iyer, K. R., Jones, J. P., Drabyshaire, J. F., and Trager, W. F. (1999) *J. Am. Chem. Soc. 21*, 41−47.
26. Harris, D., and Loew, G. (1995) *J. Am. Chem. Soc. 117*, 2738−2748.
27. Waddell, W. H., Turro, N. J., and Farrington, G. (1976) *Mol. Photochem. 7*, 475−497.
28. Fleming, G. R. (1986) in *Chemical Applications of Ultrafast Spectroscopy*, Oxford University Press, New York.
29. Unger, B. P., Gunsalus, I. C., and Sligar, S. G. (1986) *J. Biol. Chem. 261*, 1158−1163.
30. Lakowicz, J. R. (1999) *Principles of Fluorescence Spectroscopy*, 2nd ed., Kluwer Academic/Plenum Publishers, New York.
31. Lehrer, S. S. (1971) *Biochemistry 10*, 3254−3263.
32. Bankar, K. V., Bhagat, V. R., Das, R., Doraiswamy, S., Ghangrekar, A. S., Kamat, D. D., Periasamy, N., Srivastsovoy, V. J. P., and Venkateraman, B. (1989) *Indian J. Pure Appl. Phys. 27*, 416−426.
33. O'Connor, D. V., and Philips, D. (1984) *Time Correlated Single Photon Counting*, Academic Press, London.
34. Bevington, P. R. (1969) *Data Reduction and Error Analysis for the Physical Sciences*, McGraw-Hill Inc., New York.
35. Livesey, A. K., and Brochon, A. K. (1987) *Biophys. J. 52*, 693−706.
36. Jaynes, E. T. (1983) in *Papers on Probability Statistics and Statistical Physics* (Rosenkrantz, R. D., Ed.) Reidel, Dordretcht.
37. Hochstrasser, R. M., and Negus, D. K. (1984) *Proc. Natl. Acad. Sci. U.S.A. 81*, 4399−4403.
38. Cheung, H. C. (1992) *Topics in Fluorescence Spectroscopy*, Vol. 2 (Lakowicz, J. R, Ed.) pp 128−176, Plenum Press, New York.
39. Gryczynski, Z., Lubkowski, J., and Bucci, E. (1997) *Methods Enzymol. 278*, 538−569.
40. Steiner, R. F. (1991) in *Topics in Fluorescence Spectroscopy* (Lakowicz, J. R., Ed.) Vol 2, Plenum Press, New York.
41. Ehrenberg, B., and Steinberg, I. Z. (1976) *J. Am. Chem. Soc. 98*, 1293−1295.
42. Cowgill, R. W. (1967) *Biochim. Biophys. Acta 133*, 6−18.
43. Khan, K. K., Mazumdar, S., Modi, S., Sutcliffe, M., Roberts, G. C. K., and Mitra, S. (1997) *Eur. J. Biochem. 244*, 361−370.
44. Borkman, R. F., and Kearns, D. R. (1966) *J. Am. Chem. Soc. 88*, 3467−3469.
45. Sullivan, M. O., and Testa, A. C. (1970) *J. Am. Chem. Soc. 92*, 5842−5844.
46. Eftnik, M. K., and Ghiron, C. A. (1981) *Anal. Biochem. 114*, 199−227.
47. Atkins, W. M., and Sligar, S. G. (1988) *J. Biol. Chem*, *263*, 18842−18849.
48. Beechem, J. M., and Brand, L. (1985) *Annu. Rev. Biochem. 54*, 43−71.
49. Das, T. K., and Mazumdar, S. (1993) *FEBS Lett. 336*, 211−214.
50. Das, T. K., and Mazumdar, S. (1995) *Eur. J. Biochem. 227*, 823−828.
51. Szabo, A. G., Krazcar, D., Zuker, M., and Alpert, B. (1984) *Chem. Phys. Lett. 108*, 145−149.
52. Chen, R. F., Knutson, J. R., Ziffer, H., and Porter, D. (1991) *Biochemistry 30*, 5184−5195.
53. Chabbert, M., Hillen, W., Hansen, D., Takahashi, M., and Bousquet, J. A. (1992) *Biochemistry 31*, 1951−1960.
54. Watanabe, Y., and Ishimura, Y. (1989) *J. Am. Chem. Soc. 111*, 410−411.
55. Gryczynski, Z., Fronticelli, C., Tenenholz, T., and Bucci, E. (1993) *Biophys. J. 65*, 1951−1958.
56. Helms, V., Deprez, E., Gill, E., Barret, C., Hui Bon Hoa, G., and Wade, R. C. (1996) *Biochemistry 35*, 1485−1499.
57. Raag, R., and Poulos, T. L. (1991) *Biochemistry 30*, 2674−2684.
58. Raag, R., and Poulos, T. L. (1989) *Biochemistry 28*, 917−922.
59. Broos, J., Visser, A. J. W. G., Engbersen, J. F. J., Verboom, W., van Hoek, A., and Reinhoudt, D. N. (1995) *J. Am. Chem. Soc. 117*, 12657−12663.
60. Kinosita, K. J., Kawato, S., and Ikegami, A. (1977) *Biophys. J. 20*, 289−304; Lipari, G., and Szabo, A. (1980) *Biophys. J. 30* 489−494.
61. Tanford, C. (1961) *Physical Chemistry of Macromolecules*, Wiley, New York.

BI026379E